Spectrochimica Acta Part A: Molecular and Biomolecular Spectroscopy 264 (2022) 120244

Contents lists available at ScienceDirect

Spectrochimica Acta Part A: Molecular and Biomolecular Spectroscopy

journal homepage: www.elsevier.com/locate/saa

Spectroscopy of structurally disordered hydrated iron fluoridotitanate in the regions of vibrational and electronic excitations

Yu.V. Gerasimova [a,b,*], A.S. Aleksandrovsky [a,b], N.M. Laptash [c], M.A. Gerasimov [a], A.S. Krylov [a], A.N. Vtyurin [a,b], A.A. Dubrovskiy [a]

[a] Kirensky Institute of Physics, Siberian Branch of RAS, 660036 Krasnoyarsk, Russia
[b] Institute of Engineering Physics and Radio Electronics, Siberian Federal University, 660079 Krasnoyarsk, Russia
[c] Institute of Chemistry, Far Eastern Branch of RAS, 690022 Vladivostok, Russia

HIGHLIGHTS

- Raman and optical spectra of disordered hydrated iron fluoridotitanate were studied.
- Independent ordering processes of the $[TiF_6]^{2-}$ and $[Fe(H_2O)_6]^{2+}$ complexes below phase transition.
- Optical spectra are well interpretable in the Tanabe-Sugano model.
- Considerable decrease of inter-electron repulsion in the disordered neighborhood of Fe^{2+} ions is detected.

GRAPHICAL ABSTRACT

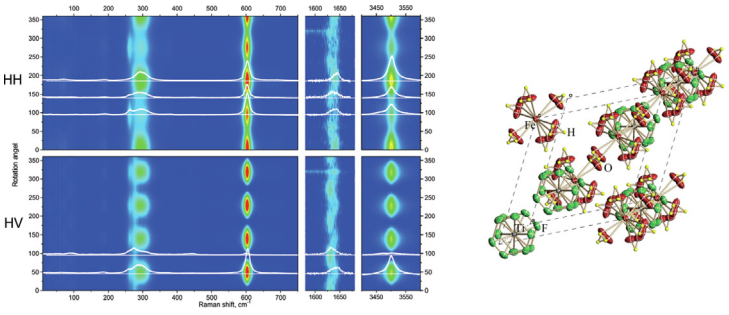

ARTICLE INFO

Article history:
Received 30 April 2021
Received in revised form 14 July 2021
Accepted 28 July 2021
Available online 31 July 2021

Keywords:
Hydrated iron fluoridotitanate
Phase transition
Order-disorder
Dynamics
Raman
Electronic excitations

ABSTRACT

Raman and optical absorption spectra of disordered hydrated iron fluoridotitanate (HITF) single crystal were studied. Temperature transformations of the Raman spectra indicate independent ordering processes of the $[TiF_6]^{2-}$ and $[Fe(H_2O)_6]^{2+}$ complexes below the structural phase transition. The absorption spectrum in the near-infrared and visible ranges includes transitions from the high spin ground state $^5T_2$ of Fe^{2+} ion to the excited ^5E state and a set of excited triplets. Analysis by Tanabe-Sugano method gives crystal field Dq = 490 cm^{-1} and Racah parameters B = 340 cm^{-1} and C = 1904 cm^{-1}. Considerable decrease of B parameter as compared to the free ion value indicates a decrease of interelectron repulsion in the disordered neighborhood of Fe^{2+} ions.

1. Introduction

Large-scale synthesis of new titanium- and iron-based multifunctional materials can be achieved through the fluoride processing of natural raw materials such as ilmenite with the idealized formula $FeTiO_3$, which is the most abundant and highly available worldwide [1,2]. Among various inorganic acids, hydrofluoric acid (HF) is the most effective for the dissolution of titanium and iron from ilmenite [3–6]. One of the main products of the interaction of ilmenite with hydrofluoric acid is hydrated iron fluoridotitanate (HITF) with the composition $FeTiF_6{\cdot}6H_20$ [7]. The compound belongs to the extensive $ABF_6{\cdot}6H_2O$ family (A = Mg, Zn, Fe, Co, Ni, Mn, Cd; B = Ti, Si, Ge, Sn, Zr), which crystallizes in a rhombohedrally distorted CsCl-type structure. Alternating $[A(H_2O)_6]^{2+}$ and $[BF_6]^{2-}$octahedra are connected with O—H···F hydrogen bonds.

* Corresponding author.
E-mail address: jul@iph.krasn.ru (Y.V. Gerasimova).

https://doi.org/10.1016/j.saa.2021.120244
1386-1425/

These compounds can be divided into two groups according to their different thermodynamic characteristics (the entropy changes at phase transitions and the signs of dT_0/dp) [8–10]. The entropy changes at phase transitions for crystals belonging to the first group is significantly larger ($\Delta S/R$ = 0.67–0.95) (A-B: Co-Si, Co-Ti, Zn-Si, Zn-Ti, Mn-Ti) compared with that for the second ($\Delta S/R$ = 0.19–0.38) (A-B: Fe-Si, Mg-Si, Mn-Si, Mg-Ti). The first group is characterized by the phase transition $R\bar{3} \leftrightarrow P2_1/c$; for the second, information on the symmetry of high-temperature and low-temperature phases is ambiguous.

Our HITF belongs to the second group and is characterized by a slight change in the entropy of the phase transition (ΔS = 1.5 J/mol K = 0.18R), which was found to be of the first order at $T_{0\downarrow}$ = 271.5 5 K, $T_{0\uparrow}$ = 274 ÷ 275.5 K with supposed symmetry transformation $P\bar{3} \leftrightarrow P\bar{1}$ in agreement with polarization-optical data [11]. However, recent single crystal X-ray analysis showed that the room temperature (RT) structure of the crystal belongs more preferentially to $R\bar{3}$ group and transforms into $P2_1/c$ upon cooling [12]. It should be noted that the low-temperature (LT) phase of HITF in both space groups ($P2_1/c$ and $P\bar{1}$) are virtually the same in structure within the error limits. The cationic sublattice of the crystal includes a certain amount of $[Fe^{3+}(H_2O)_5F]^{2+}$, and $[Ti^{3+}(H_2O)_5F]^{2+}$, and the anionic sublattice includes a certain amount of hydroxide ions instead of fluoride so that the real composition of the crystal corresponds to the formula $Fe_{0.9}Ti_{1.1}(OH)_{0.5}F_{5.7}\cdot 5.8H_2O$. For simplicity, we will use the stoichiometric formula $FeTiF_6\cdot 6H_2O$ or the abbreviation HITF.

Detailed knowledge of the lattice dynamics is necessary to reveal the microscopic mechanism of phase transition in HITF. Raman measurements at different temperatures can provide valuable information about this mechanism including the bonding and dynamics of water molecules and also clarify some disagreement between the optical and X-ray structural data of the LT phase of HITF.

2. Experimental details

The synthesis and composition of high-quality yellowish-green crystals of HITF were described earlier [13,14]. We used a prismatic crystal elongated along the *c* axis (Fig. 1).

Polarized Raman spectra have been obtained with triple spectrometer Jobin Yvon T64000 equipped with a liquid nitrogen-cooled charge-coupled device (CCD) detection system in subtractive dispersion mode using backscattering geometry. Absorption spectra in the region of electronic excitations were recorded using Shimadzu UV-3600 spectrometer with a resolution of 0.5 nm.

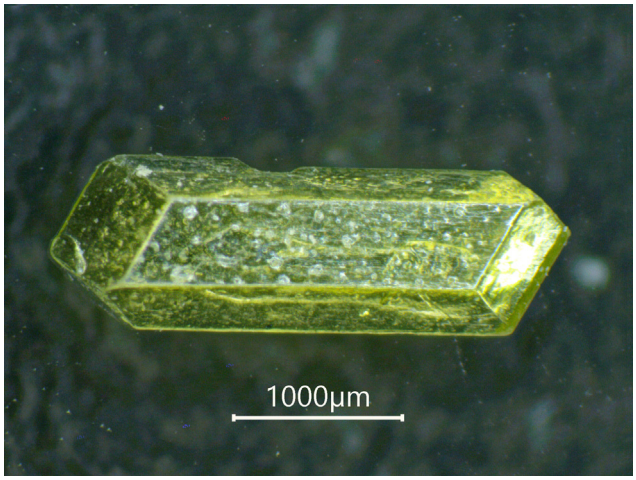

Fig. 1. Single crystal of $FeTiF_6\cdot 6H_2O$.

The spectral resolution of Raman spectra using gratings with 1800 mm^{-1} grooves and 100 μ slits) was about 2 cm^{-1} (The micro-Raman system is based on an Olympus BX41 microscope with a 50× objective lens *f* = 1.2 mm with numerical aperture N. A. = 0.75 provides a focal spot 4 μm diameter on the sample. Single-mode λ = 532 nm radiation from an Excelsior diode-pumped CW laser (Spectra-Physics) of 3 mW on the sample was used as an excitation light source.

Two experiment series were conducted with parallel and crossed polar polarizations of the incident and scattered beams to study the angular dependence of intensities of Raman spectra. Backscattering geometry was used. The shift of the incidence point of exciting radiation was not more than 2 μm on a complete 2π revolution.

Temperature measurements were performed with a closed-cycle ARS CS204-X1.SS helium cryostat in the temperature range of 8–400 K. The temperature was monitored by LakeShore DT-6SD1.4L silicon diode. During experiments, the cryostat was evacuated to 1×10^{-6} mbar. Spectroscopic measurements were performed in the subtractive dispersion mode, which attained a low-wavenumber limit of 10 cm^{-1} in the present setup for investigation of the low-wavenumber spectra.

3. Results and discussion

3.1. Spectroscopy of electronic excitations

The absorption spectrum of $FeTiF_6\cdot 6H_2O$ at room temperature is presented in Fig. 2.

In the RT crystal structure of HITF with space group $R\bar{3}$ (C_{3i}), isolated disordered octahedra $[Fe(H_2O)_6]^{2+}$ and $[TiF_6]^{2-}$ are distributed over two orientations around the 3-fold axis. The ligands disorder between two positions is of equal occupancy. The Fe—O distances in octahedrons are equal to 2.107–2.108(2) Å. The octahedral local environment is known to be most favorable for the manifestation of the Jahn-Teller effect that could be observed like splitting of the absorption line at spin-allowed transition [13]. However, the spectrum in Fig. 2 is featured by a single strong peak centered at 1940 nm (0.64 eV) that is consistent with the assumption that the ground state of Fe^{2+} in the local environment specified above is a high-spin one, namely, $^5T_2$. Strong absorption in the vicinity of 1940 nm is then assigned to the spin-allowed transition from high-spin ground state $^5T_2$ to excited state ^5E. This assignment is supported by numerous measurements of Fe^{2+} spectra in various crystals, including FeF_2 [13]. However, in FeF_2 local symmetry of the Fe^{2+} ion is cubic, and consequently, splitting between $^5T_2$ and ^5E here is expected to be stronger in FeF_2 than in $FeTiF_6\cdot 6H_2O$. The absorption bands observed in $FeTiF_6\cdot 6H_2O$ in the rest of the NIR-VIS range are much weaker than the $^5T_2$ – ^5E band, and therefore, they could be assigned to the Fe^{2+} absorption at spin-forbidden ions as well as the absorption from ions with deviated valence earlier detected in the material under study via XPS [14], that is Fe^{3+} and Ti^{3+}.

To check the validity of the band assignments in the $FeTiF_6\cdot 6H_2O$ absorption spectrum to the energy levels of Fe^{2+} ion, the fitting of experimental energies of transitions to the theoretical positions of energy levels calculated with the help of the Tanabe-Sugano approach was done. The best fit was obtained for the crystal field strength Dq = 490 cm^{-1} and Racah parameters B = 340 cm^{-1} and C = 1904 cm^{-1} (Dq/B = 1.44). Tanabe-Sugano diagram for d^6 electron configuration at the optimized values B and C are presented in Fig. 3. The comparison between experimental and calculated energies of levels is presented in Table 1.

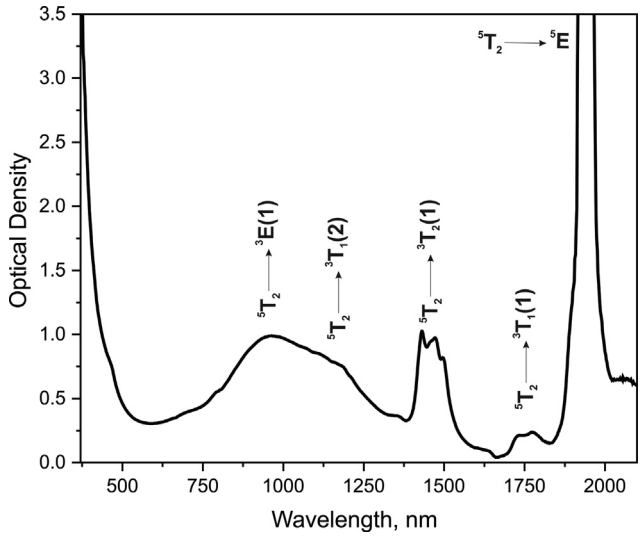

Fig. 2. The unpolarized absorption spectrum of $FeTiF_6{\cdot}6H_2O$ crystal in the region of *d-d* electronic excitations.

Table 1
Observed and fitted energy states of Fe^{2+} ion in $FeTiF_6{\cdot}6H_2O$.

Energy levels	Observed Energy (cm^{-1})	Calculated Energy (cm^{-1})
$^5T_2 \rightarrow {}^5E$	5155	4900
$^5T_2 \rightarrow {}^3T_1(1)$	5682	5390
$^5T_2 \rightarrow {}^3T_2(1)$	6897	6943
$^5T_2 \rightarrow {}^3T_1(2)$	8696	9425
$^5T_2 \rightarrow {}^3E(1)$	10,300	10,619
$^5T_2 \rightarrow {}^3T_1(6)$	~22,200	23,733

Table 2
Raman frequencies (cm^{-1}) observed in different polarizations.

HV(R)	HH (R)	assignment
	68	–
188	188	Restricted H_2O translation
261	–	ν_{as} (Fe—O)
295	293	$\delta(TiF_6) - \nu_5$
602	602	ν_s (TiF_6) – ν_1
1636, 1648	1636, 1648	δ (H_2O)
3500	3500	ν_{as} (H_2O)

As one can see from Table 1, the absorption spectrum of $FeTiF_6{\cdot}6H_2O$ can be fairly explained by the absorption at the spin-allowed transition and transitions to triplets of Fe^{2+} ions only, while transitions to singlet states can be expectedly ruled out from the consideration due to their weak oscillator strengths concerning those to the triplet states. Rather low fitted value of Racah parameter B = 340 cm^{-1} that is much lower than B parameter for free Fe^{2+} ion evidence noticeable decrease of the inter-electronic repulsion in the specific local environment of this ion within the crystal under study. It can be explained either by the dynamic disorder of the environment or by the presence of hydrogen in the second coordination sphere; the second explanation looks more preferable Table 2.

3.2. Temperature dependence of the Raman modes and the phase transition mechanism

The angular dependences of the Raman spectra of an unoriented sample make it possible to assign the lines to irreducible representations of the corresponding space group. Different representations will have different patterns of angular dependences on the intensities of the Raman spectra (Fig. 4). Experimental details of this technique were given in [15,16].

The $[TiF_6]^{2-}$ is a regular octahedron having O_h molecular symmetry; its 15 internal vibrational modes belong to the representations $A_{1g} + E_g + F_{2g} + 2F_{1u} + F_{2u}$ where modes A_{1g}, E_g, F_{2g} are Raman active. According to [17] the line at 602 cm^{-1} corresponds to the A_{1g} mode of $[TiF_6]^{2-}$ complex, the E_g mode should show at

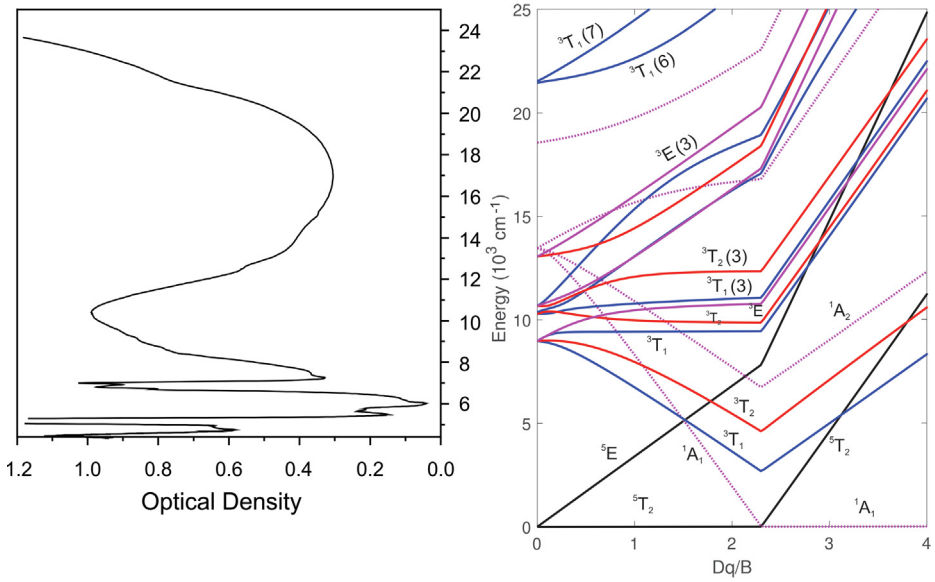

Fig. 3. Tanabe-Sugano diagram for d^6 electronic system at Racah parameters B = 340 cm^{-1}, C = 1904 cm^{-1} (right panel). $^5T_2$ and ^5E levels are drawn by black lines, triplet states are drawn by blue ($^3T_1$), red ($^3T_2$), and magenta (^3E) lines. Dotted lines correspond to singlet states. The absorption spectrum of $FeTiF_6{\cdot}6H_2O$ in the energy scale is drawn at the left panel for comparison.

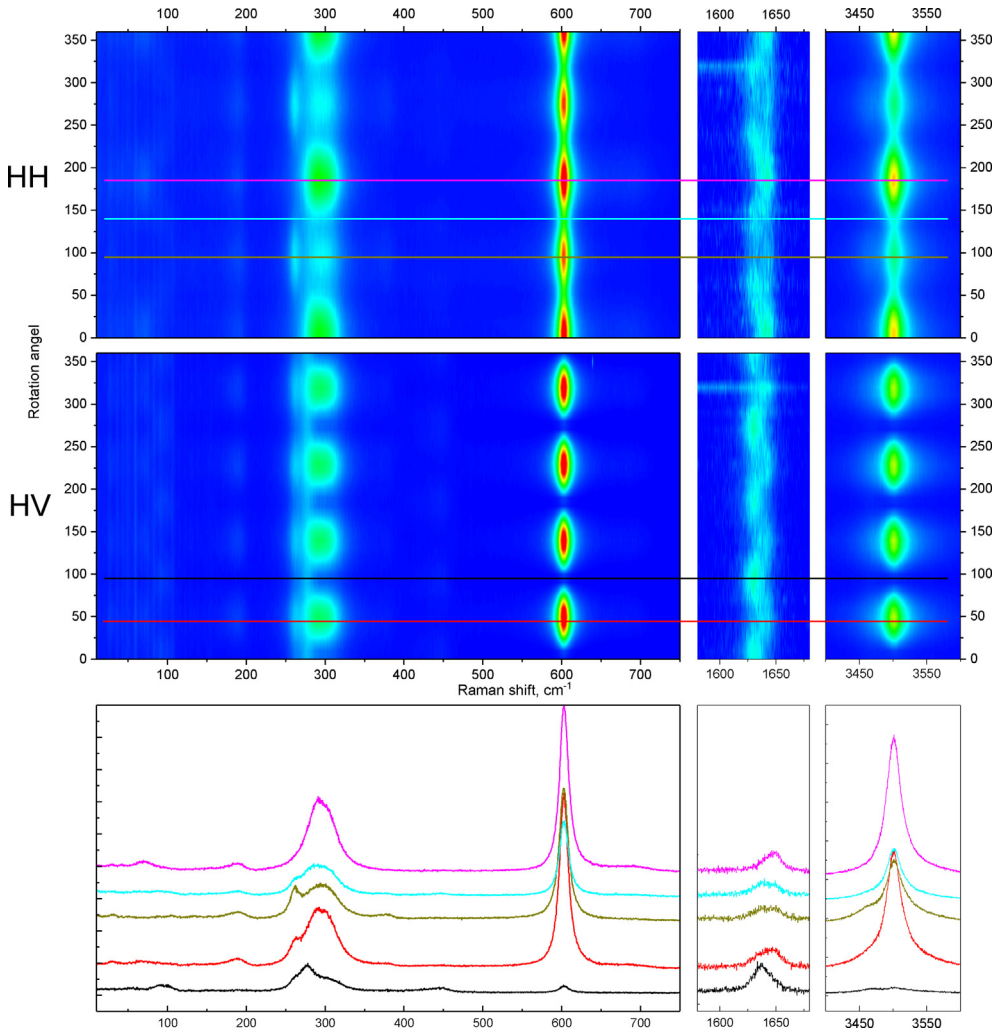

Fig. 4. Angular Raman spectrum of $FeTiF_6{\cdot}6H_2O$ at room temperature. H direction along long crystal axis (*c*).

440 cm^{-1}, but it does not appear there due to very small intensity, and the F_{2g} mode appears at 300 cm^{-1}.

There are the following 51 normal modes for the complex $[Fe(H_2O)_6]^{2+}$ of T_h symmetry: $3A_g + A_u + 3E_g + E_u + 5F_g + 8F_u$ [18–21]. Corresponding frequencies of Raman lines at different scattering geometries are given in Table 2, while Raman spectra at different geometries and intensity maps are shown in Fig. 4; colors of graphs correspond to the colors of sections on the map.

The most intense line in crossed HV polarization at 602 cm^{-1} (A_{1g}) shows four equal maxima on the map. Such angular distribution of Raman intensity confirms the *c* axis orientation of the sample. Lines with the same pattern at the intense map are supposed to belong to the same symmetry representation. That is the line at 3500 cm^{-1} while the contour at 293 cm^{-1} refers to the mode of F_{2g} symmetry.

Temperature transformations of the spectra are shown in Figs. 5 and 6. Experimental spectra don't show rightly the phase transition observed in [11], so to fix its temperature we've measured sample capacity with the PPMS 9 T (see Fig. S1).

A set of low frequency lines appears in a 0–130 cm^{-1} range [22] that correspond to librational modes of the complex groups (see Fig. S2). Such sharp and narrow rotational lines indicate the rotational ordering of that complexes.

At room temperature in the $R\bar{3}$ phase internal modes of octahedral complexes are rather wide and weak lines are covered by wings of the intense ones. The evolution of these lines becomes visible undercooling and we can see the appearance of weaker lines at 400–500 cm^{-1} and 706 cm^{-1} that correspond to librations of H_2O molecules. The single line corresponding to the full symmetry mode of the $[TiF_6]^{2-}$ complex becomes narrow at lower temperatures (dependence of half-width of this line vs. temperature is shown in extra materials S3). Five lines appear near 300 cm^{-1} in the lower temperature phase that correspond to the triple degenerate $\delta(TiF_6)$ mode and the ν_{as}(Fe—O) one (Fig. 6).

The stretching line of the water molecule at 3500 cm^{-1} splits into a doublet below 100 K (Figs. 5 and 6) that evidences the ordering of water containing octahedrons with the reconstruction of O—H···F hydrogen bonds. According to crystallographic data [12], all hydrogen bonds in the LT structure are approximately the same, the O···F distances lie in the range of 2.74–2.77 Å, while in the RT structure they are distributed into three groups: d(O···F) = 2.69, 2.75 and 2.83 Å. The O···F bonds with d = 2.75 Å link the $[TiF_6]^{2-}$ and $[Fe(H_2O)_6]^{2+}$ octahedra into chains along the *c* axis, and the O···F bonds with d = 2.69 Å join the chains into layers parallel to the (1 1 0) plane. The O···F bonds at 2.83 Å are realized between polyhedron atoms of different orientations. Despite the different system of hydrogen bonds in the RT phase of HITF, the stretching vibration of water appears as one relatively wide line due to the dynamic disorder in the cation sublattice, while it appears as symmetric and asymmetric stretching vibrations during ordering in the LT phase.

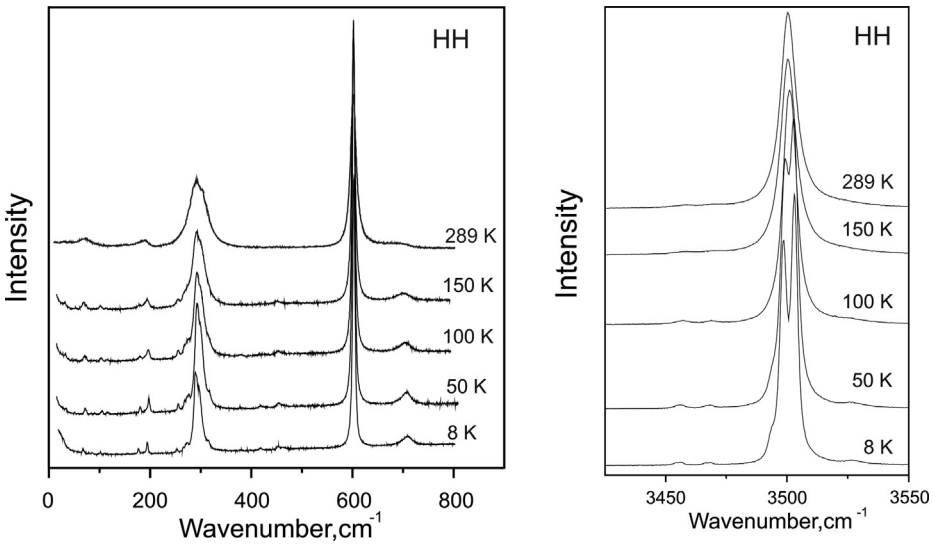

Fig. 5. Raman spectra of $FeTiF_6{\cdot}6H_2O$ in the range of $[TiF_6]^{2-}$ and complex $[Fe(H_2O)_6]^{2+}$ at different temperatures (HH polarization).

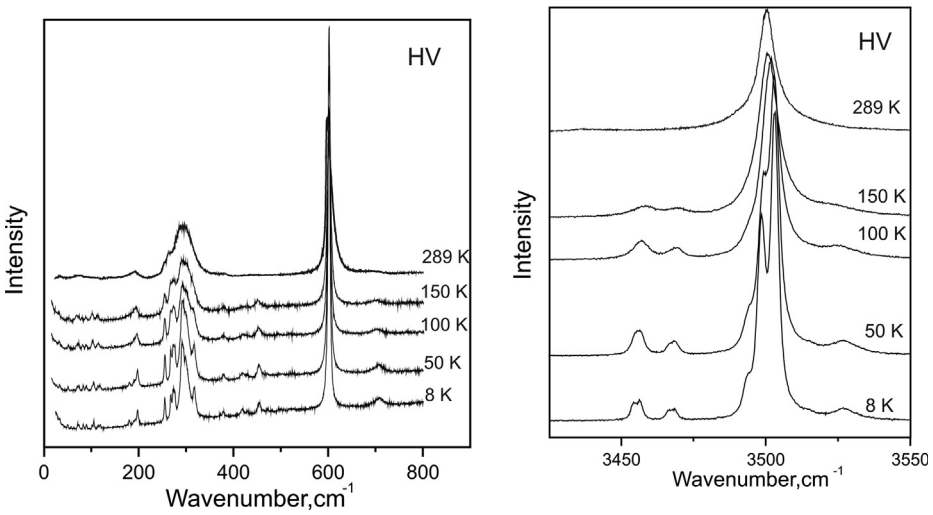

Fig. 6. Raman spectra of $FeTiF_6{\cdot}6H_2O$ in the range of $[TiF_6]^{2-}$ and complex $[Fe(H_2O)_6]^{2+}$ at different temperatures (HV polarization).

It should be noted that the change from trigonal symmetry with rapid reorientational motions to monoclinic symmetry without these motions with the rearrangement of hydrogen bonds has been found in most of the fluoridotitanates [23–25]. However, the assumption about the rotation of fluorooctahedral ions in the LT phase around the C_3 axis was made for $MgTiF_6{\cdot}6H_2O$ [25]. Choudhury et al. studied phase transitions in $ZnTiF_6{\cdot}6H_2O$ and $MnTiF_6{\cdot}6H(D)_2O$ by Raman spectroscopy to see whether the distortions of the two octahedra are independent or there is a coupling between them [26–28].

In the crystal under our investigation temperature transformations of Raman lines indicate that both $[TiF_6]^{2-}$ and $[Fe(H_2O)_6]^{2+}$ complexes are orientationally disordered in the high temperature phase. $[TiF_6]^{2-}$ complexes start ordering just below the transition point while ordering of $[Fe(H_2O)_6]^{2+}$ complexes follows at much lower temperatures, around 100 K.

4. Conclusions

Structural ordering of complex $[TiF_6]^{2-}$ and $[Fe(H_2O)_6]^{2+}$ octahedrons has been studied by VIS absorption and Raman spectroscopy. Absorption spectra of Fe^{2+} ions do not show any Jahn-Teller splitting in the disordered room temperature phase. The spectra have been analyzed using the Tanabe-Sugano approach. They agree quite well within the *d-d* transitions model for d^6 configuration with Dq = 490 cm^{-1} and Racah parameters B = 340 cm^{-1} and C = 1904 cm^{-1} (Dq/B = 1.44) and without alternating valence of iron ions. Obtained Raman data provide new informaion on phase transition mechanism in the studied crystal. Ordering of both $[TiF_6]^{2-}$ and $[Fe(H_2O)_6]^{2+}$ complexes were observed, but independently. Groups $[TiF_6]^{2-}$ becomes ordered just below the thansition point while ordering of $[Fe(H_2O)_6]^{2+}$ follows far below after forming stable O-H. . .F hydrogen bonds.

CRediT authorship contribution statement

Yu.V. Gerasimova: Conceptualization, Investigation, Writing – original draft. **A.S. Aleksandrovsky:** Investigation. **N.M. Laptash:** Writing - original draft. **M.A. Gerasimov:** Investigation. **A.S. Krylov:** Methodology, Data curation. **A.N. Vtyurin:** Validation, Writing – review & editing.

Declaration of Competing Interest

The authors declare that they have no known competing financial interests or personal relationships that could have appeared to influence the work reported in this paper.

Acknowledgments

The reported study was funded by Russian Foundation for Basic Research, Government of Krasnoyarsk Territory and Krasnoyarsk Regional Foundation of Science according to the research project "Spectral and magnetic properties of single crystals of transition metal fluoride hexahydrates." No. 20-42-240014.

Appendix A. Supplementary material

Supplementary data to this article can be found online at https://doi.org/10.1016/j.saa.2021.120244.

References

[1] A. Dubenko, M.V. Nikolenko, A. Kostyniuk, B. Likozar, Sulfuric acid leaching of altered ilmenite using thermal, mechanical and chemical activation, Minerals 10 (2020) 538.
[2] T.K. Pong, J. Besida, T.A. O'Donnell, D. Wood, A novel fluoride process for producing TiO_2 from titaniferous ore, Ind. Eng. Chem. Res. 34 (1995) 308–313.
[3] R.K. Biswas, M.G.K. Mondal, A study on the dissolution of ilmenite sand, Hydrometallurgy 17 (3) (1987) 385–390.
[4] D.A. Hansen, D.E. Traut, The kinetics of leaching rock ilmenite with hydrofluoric acid, JOM –, J. Miner. Metals Mater. Soc. 41 (5) (1989) 34–36.
[5] R.K. Biswas, M.A. Habib, N.C. Dafader, A study on the recovery of titanium from hydrofluoric acid leach solution of ilmenite, Hydrometallurgy 28 (1992) 119–126.
[6] M.H. Rodrigues, G.D. Rosales, F.M. Pinna, N.T. Tunez, Extraction of titanium from low-grade ore with different leaching agents in autoclave, Metals 10 (2020) 497.
[7] N. Keisuke, Y. Hideyuki, H. Toshio, K. Takaho, Method for producing titanium fluoride, EP 0319857 A1, Eur. Patent (1989).
[8] I.N. Flerov, M.V. Gorev, S.V. Melnikova, M.L. Afanasyev, K.S. Aleksandrov, Study of phase transitions in $ABF_6{\cdot}6H_2O$ crystals, Fiz. Tverd. Tela 33 (1991) 1921–1929.
[9] I.N. Flerov, M.V. Gorev, K.S. Aleksandrov, M.L. Afanasyev, Effect of hydrostatic pressure on phase transitions in ABF6·6H2O crystals (A = Zn Co, Mg, Mn, Fe B = Ti, Si), J. Phys.: Condens. Mater. 4 (1992) 91–99.
[10] I.N. Flerov, M.V. Gorev, S.V. Melnikova, M.L. Afanasyev, K.S. Aleksandrov, Investigations of ferroelastic phase transitions in ABF6·6H2O crystals (A: Zn Co, Mg, Mn, Fe; B: Ti, Si), Ferroelectrics 143 (1993) 11–16.
[11] S.V. Mel'nikova, N.M. Laptash, M.V. Gorev, E.I. Pogoreltsev, Mixed-valence hydrated fluoridotitanate: Synthesis, optics and calorimetry, J. Phys. Chem. Solids 142 (2020) 109444.
[12] A.A. Udovenko, E.A. Goreshnik, E.B. Merkulov, N.M. Laptash, Mixed-valence hydrated iron fluoridotitanate: Crystal structure and thermal behavior, J. Fluorine Chem. (2021) 109853.
[13] T. Tsuboi, W. Kleemann, The optical exciton-magnon absorption lines in FeF_2 crystals, J. Phys. Cond. Matt. 5 (8) (1993) 1151–1168.
[14] J. Tylicki, W.M. Yen, Magnetic effects in the near-Infrared spectrum of FeF_2, Phys. Rev. A 166 (1968) 488–494.
[15] Aleksandr S. Oreshonkov, Julia V. Gerasimova, Alexandr A. Ershov, Alexander S. Krylov, Kirill A. Shaykhutdinov, Aleksandr N. Vtyurin, Maxim S. Molokeev, Konstantin Y. Terent'ev, Natalia V. Mihashenok, Raman spectra and phase composition of $MnGeO_3$ crystals, J. Raman Spectrosc. 47 (5) (2016) 531–536.
[16] Ying Chang, Aixia Xiao, Rubing Li, Miaojing Wang, Saisai He, Mingyuan Sun, Lizhong Wang, Qu. Chuanyong, Wei Qiu, Angle-Resolved Intensity of Polarized Micro-Raman Spectroscopy for 4H-SiC, Crystals 11 (2021) 626.
[17] K. Nakamoto, Infrared and Raman Spectroscopy of Inorganic andCoordination Compounds: Applications in Coordination,Organometallics and Bioinorganic Chemistry, John 6th Wiley and Sons, United States, 2009.
[18] P. Choudhury, B. Ghosh, G.S. Raghuvanshi, H.D. Bist, The Raman spectra of manganese and zinc fluorotitanate hexahydrate systems, J. Raman Spectrosc. 14 (1983) 99–101.
[19] John Lewis, Tudor E. Jenkins, The Raman spectra of some hexa-aquo metal(II) hexafluorosilicate(IV) ($M(H_2O)_6SiF_6$) salts between 10 K and 300 K, J. Raman Spectrosc. 8 (2) (1979) 111–114.
[20] Ichiro Nakagawa, Takehiko Shimanouchi, Infrared absorption spectra of aquo complexes and the nature of coordination bonds, Spectrochim. Acta 20 (3) (1964) 429–439.
[21] T.E. Jenkins, J. Lewis, Raman investigation of some metal (II) hexafiuorosilicate (IV) and hexafluorotitanate (IV) salts, Spectrochim. Acta A 37 (1981) 47–50.
[22] V.V. Eremenko, A.V. Peschanskii, V.I. Fomin, Raman scattering in crystalline fluorosilicate hexahydrates of iron and manganese at a phase transition, Phys. Solid State 39 (1997) 830–839.
[23] M. Bose, K. Roy, A. Ghoshray, ^2H NMR studies of structural phase transitions in some members of the deuterated $ABF_6{\cdot}6H_2O$ system, Phys. Rev. B 35 (1987) 6619–6626.
[24] R.L. Lichti, I.-Y. Jan, K.G. Casey, Phase transitions in the (Ni, Zn)$Ti_F6{\cdot}6_H20$ system, J. Solid State Chem. 78 (1989) 250–255.
[25] E.P. Zeer, O.V. Falaleev, Yu.N. Ivanov, E.A. Petrakovskaya, Study of molecular mobility in crystals of the $ABF_6{\cdot}6H_2O$ family, Fiz. Tverd. Tela 36 (1994) 2210–2220.
[26] P. Choudhury, B. Ghosh, M.B. Patel, H.D. Bist, The phase transition and the mode-coupling phenomenon observed in $MnTiF_6.6D_2O$ using Raman scattering, J. Phys. C: Solid State Phys. 17 (32) (1984) 5827–5832.
[27] P. Choudhury, B. Ghosh, M.B. Patel, H.D. Bist, Phase transition in manganese and zinc fluorotitanate h hexadeuterate systems observed by Raman spectroscopy, J. Raman Spectrosc. 16 (1985) 149–155.
[28] A.N. Das, P. Choudhury, B. Ghosh, An explanation of the change in frequency and linewidth of the symmetric stretching vibration $v_s(H_20)$ in $ZnTiF_6{\cdot}6H_2O$ and $MnTiF_6{\cdot}6H_2O$ near the transition point, J. Phys. C: Solid State Phys. 18 (1985) 5975–5986.